

Bearing Capacity of Reinforced Horizontal Sandy Ground

Ching-Chuan Huang & Fumio Tatsuoka

Institute of Industrial Science, University of Tokyo, Minato-ku, Japan

ABSTRACT

In order to develop a method of predicting the bearing capacity of horizontal sandy ground reinforced with tensile-reinforcement layers horizontally placed beneath a footing, a series of plane strain model tests with a strip footing was performed. The effects of the length, the arrangements and the rigidity and rupture strength of reinforcement were examined systematically. The strain fields in sand, the tensile forces in reinforcement and the distribution of contact pressure on footing were measured.

Even by means of reinforcement layers with a length similar to the footing width, the bearing capacity increased remarkably. Also, the portions of reinforcement layers located outside the footing width contributed to the increase in the bearing capacity only in a secondary way. The bearing capacity of reinforced sand was found equal to the smaller of the following two values; the one controlled by the failure of the reinforced zone immediately beneath the footing and the other by the failure of sand beneath the reinforced zone.

Based on the test results, a method of stability analysis by the limit equilibrium method was developed, taking into account the effects of the arrangement and properties of reinforcement and the failure modes of reinforced sand. The predicted values were well in accordance with the measured ones.

NOTATION

A_R	cross-sectional area of reinforcing strip
B	width of footing (=10 cm)

BCR	bearing capacity ratio = {increased value of q_u by deepening footing or by reinforcing}/{ q_u for surface footing on unreinforced sand}
CR	covering ratio, or plane density of reinforcement
D	depth of each reinforcement layer
D_f	depth of footing
D_R	depth of the deepest reinforcement layer
E_R	Young's modulus of reinforcement
L	length of reinforcement
n	number of reinforcement layers
$N = 2q/(\gamma_d \cdot B)$	normalized contact pressure on footing
$N_{\gamma q}$	the maximum value of N
q	average contact pressure
q_u	peak value of q
S	settlement of footing
S_f	settlement of footing at peak load
S_R	horizontal spacing of reinforcement
W	width of reinforcement member
γ_d	dry unit weight of sand
ε_1	major principal strain (%)
ε_2	intermediate principal strain (%)
ε_3	minor principal strain (%)

1 INTRODUCTION

In some engineering practices, the bearing capacity of ground has to be improved in an economical way. One of the promising methods is to place tensile-reinforcement layers horizontal beneath the footing.

For reinforced sandy ground loaded with a footing, the following two different failure mechanisms have been proposed:

(1) An anchoring mechanism (Binquet & Lee^{1,2}); the reinforcement layers should be sufficiently longer than the footing width so that the portions anchored in the zones outside the footing width can resist the downwards displacement of the zone immediately beneath the footing (Fig. 1).

(2) A strain-restraining mechanism (Huang & Tatsuoka³); the reinforcement layers having a length similar to the footing width can remarkably increase the bearing capacity by increasing the compressive strength of the reinforced zone immediately beneath the footing, as a result of restraining potential tensile strains in that zone.

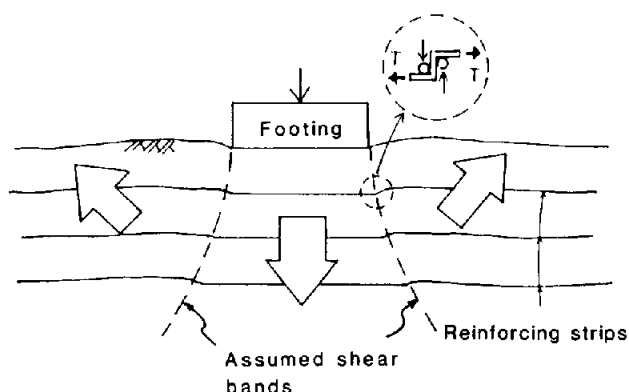


Fig. 1. Anchoring failure mechanism.

The above two mechanisms lead to totally different design procedures. Thus, the present study was performed:

- (1) to obtain a fundamental understanding of the failure mechanism of reinforced sand loaded with a surface footing,
- (2) to examine experimentally the effects of the length, the number of layers, the horizontal spacing and the stiffness and rupture strength of reinforcement, and
- (3) to develop a rational method of stability analysis, suitable for designing.

The tests were performed on level, model sandy ground. However, it was considered that the findings obtained from the present study may be applied to the case of a footing placed near the slope of embankment after some modifications. A part of the results of the present study has been reported elsewhere.³

2 MODEL TEST

Figure 2 shows the setup of the model test. Each side wall of the sand box consisted of a 3 cm-thick transparent acryl plate, restrained by a steel stiffener for ensuring the plane strain condition. The inside surface of the acryl plate was well lubricated by means of a 0.5 mm-thick silicone grease layer placed between the plate and a 0.2 mm-thick latex rubber membrane in contact with sand. The friction angle in the zone beneath the footing under the test condition, estimated from the direct shear tests on the lubrication layers, was about 0.05° .⁴

On the outer surface of the membrane, 1 cm-square meshes were

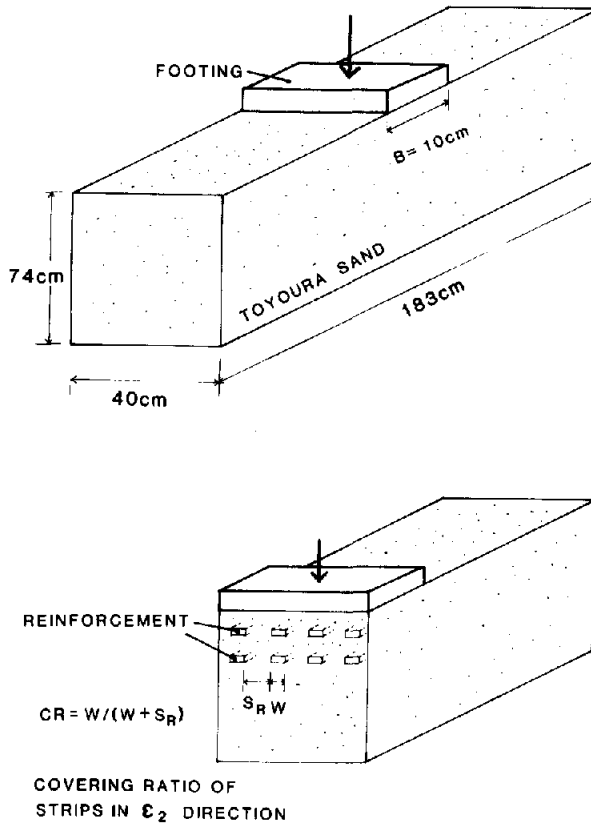


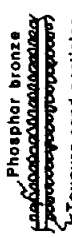
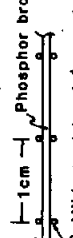
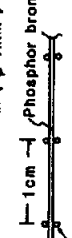
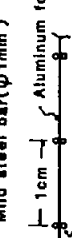
Fig. 2. Model test arrangement.

drawn. Displacements in the intermediate principal strain (ϵ_2) plane in the model were obtained from displacements at the nodes of the meshes. They were read from pictures taken occasionally during each test. It has been confirmed that the displacements in the model seen in the lateral surface are virtually the same as those at the central section.

Each model ground was constructed by pluviating air-dried Toyoura sand from a slit of a hopper, which was moved over the sand box repeatedly. The falling height was adjusted so that it was kept between 80 and 82 cm. By this method, homogeneous sand models having relative density values in a range of 80~86% were obtained. At each prescribed depth, pluviating of sand was temporarily ceased and a layer of reinforcement was placed on the surface of sand. After this, sand pluviating was continued.

Toyouura sand has a mean diameter of 0.16 mm, a coefficient of uni-

TABLE 1
List of Model Reinforcement Members

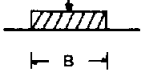
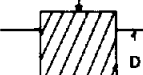
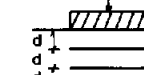
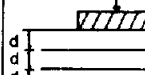

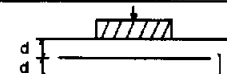
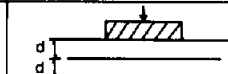
Type of reinforcing strip	Schematic figure	Thickness (cm)	Width (cm)	Length (cm)	Cross sectional area A_R (cm ²)	Elastic modulus (kN/m ²)	Tensile strength (kN/strip)
Type-1	 Phosphor bronze Toyourea sand particles 1cm	0.05	0.3	1B-6B	0.015	1.22×10^8	350
Type-2	 Phosphor bronze Mild steel bar (ϕ 1mm) 1cm	0.05	0.3	2B	0.015	1.22×10^8	350
Type-3	 Phosphor bronze Mild steel bar (ϕ 1mm) 1cm	0.01	0.3	2B	0.003	1.22×10^8	70
Type-4	 Aluminum foil Mild steel bar (ϕ 1mm) 1cm	0.005	0.3	2B	0.0015	0.7×10^8	17

formity of 1.46, a specific gravity of 2.64 and a sub-angular to angular particle shape, with a high content of quartz. The maximum and minimum values of dry unit weight γ_d determined by the method specified by the Japanese Society of Soil Mechanics and Foundation Engineering are 16.11 and 13.09 kN/m³. The plane strain strength and deformation properties of Toyoura sand have been thoroughly studied.^{5,6}

A 10 cm-wide rigid footing with a rough base, guided against tilting, was loaded at a controlled displacement rate between 0.1 and 0.2 mm/min. The normal and shear stresses and their distributions were measured at the central third of strip footing by means of five load cells, each of which measured the normal and shear forces separately.

Four types of reinforcing strips were used (Table 1). The tensile rigidity $E_R \cdot A_R$ and the rupture strength of reinforcement were changed largely to study their effects. Except for Type-4, the tensile forces in reinforcement were measured by means of strain gages attached to their surfaces. The surfaces of all the reinforcements were made very rough. For Types-1, 2 and 3, the particles of Toyoura sand were glued to the surfaces and for Type-4, ribs of mild steel bar with a diameter of 1 mm were attached at a spacing of 1.0 cm.

The tests performed are listed in Table 2. They consist of the following five groups (see Fig. 3):

Group-a			Group-b	
				
$D_f = 80, 83, 86(\%)$ relative density	$D_f = 0.3B, 0.6B,$ $0.9B, 1.5B$	$D_R = 0.3B, 0.6B,$ $0.9B, 1.5B$	$n = 3$ $L = 1.0B, 2.0B, 3.5B,$ $6.0B$	
Group-c		Group-d		Group-e
				
$n = 1, 2, 3$ $L = 6B$		$n = 3$ $L = 2B$ $CR = 4.5\%, 9.0\%, 18\%$		$n = 3$ $L = 2B$ $E_R \cdot A_R = 18.3, 3.66,$ $1.05 (\times 10^4) \text{ N}$

n : number of reinforcement layers , $d/B = 0.3$

Fig. 3. Groups of tests.

Group-a: to study whether short reinforcement layers having a length L similar to the footing width B can reinforce the ground effectively. The purposes include also the effects of the number of layers of the short reinforcement with $L = B$. Three tests with a footing on the surface on unreinforced sand were performed as reference tests. In the tests of Group-a through Group-d, only Type-1 reinforcement was used.

Group-b: to study into the effects of the length of reinforcement, $L = B, 2B, 3.5B$ and $6B$, in the case of the number of layers $n = 3$. Only in Test No. 18, the length was not constant as $L = 2B$ for the topmost layer and $3.5B$ for the other lower layers.

Group-c: to study into the effects of the number of layers, $n = 1, 2$ and 3 , in the case of long reinforcement of $L = 6B$.

Group-d: to study into the covering ratio CR , in the case of $L/B = 2$ and $n = 3$. CR is defined in Fig. 2.

Group-e: to study into the effect of the rigidity and rupture strength of reinforcement in the case of $L/B = 2$ and $n = 3$. In this group, all the types of reinforcement were used.

3 TEST RESULTS

3.1 Group-a

Figure 4 shows the normalized relationships between footing load and settlement for Group-a, in terms of $N = 2q/(\gamma_d \cdot B)$ and S/B . The values of N in this and the following similar figures are not corrected for the differences in γ_d among different tests. It may be seen that even short reinforcement of $L = B$ can increase both the initial stiffness and peak strength of ground.

It may also be seen that the bearing capacity for sand reinforced to a depth of D_R with $CR = 18\%$, loaded with a surface footing, is very similar to that of the unreinforced sand, loaded with a rigid deep footing having the same depth $D_f = D_R$. This is the case for $D_f = D_R$ up to $0.9B$. However, the sand reinforced to $D_R = 1.5B$ had a lower initial stiffness than the deep footing with $D_f = 1.5B$, while the peak strengths in both the cases were very similar.

For both unreinforced and reinforced cases, with the increase in the depth (i.e., D_f and D_R), the settlement at peak (S_f) increased. This is due to higher compressibilities of the sand at higher pressure levels, as has been observed in the plane strain compression (PSC) test on Toyoura sand.⁴ A larger value of S_f in the reinforced sand of $D_R = 1.5B$ than the unreinforced sand loaded with a deep footing of $D_f = 1.5B$ may be due to

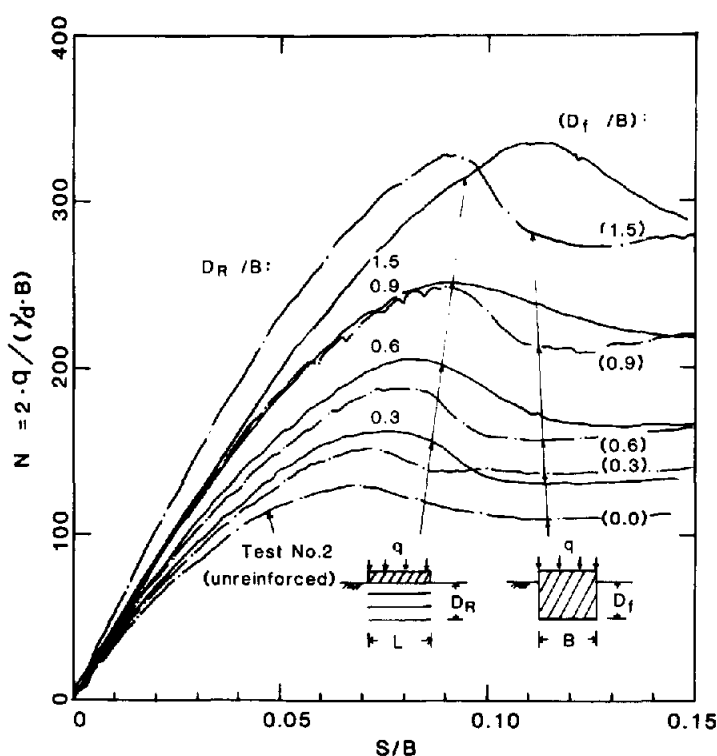


Fig. 4. Footing load-displacement relations for Group-a.

compression in the reinforced zone caused by the increased footing load.

Figure 5(a) shows the contours of maximum shear strain $\varepsilon_1 - \varepsilon_3$ between the start of loading and $S_f = 0.07B$ at which the failure for the unreinforced sand of $D_f = D_R = 0$ occurred. This figure was constructed from the corresponding strain field, obtained as follows. The strain at the center of each $1 \text{ cm} \times 1 \text{ cm}$ element was obtained from the displacements at its four nodes measured from its picture, assuming a linear variation in strain in the element. The accuracy for displacements estimated was about 0.012 mm and that for strains was about 1.0% .

Intensely sheared bands appeared from the edges of the footing and a wedge was formed immediately beneath the footing. Outside and inside the wedge, strains remained relatively small. Note that at the failure of sand (i.e., when the peak strength or the angle of internal friction $\phi = \arcsin\{(\sigma_1 - \sigma_3)/(\sigma_1 + \sigma_3)\}_{\max}$ is mobilized), the maximum shear strain ($\varepsilon_1 - \varepsilon_3$) in a plain strain compression (PSC) test is about 5% under the same test condition of the present study. This result indicates that the failure in sand is rather progressive in the sense that the peak strength is

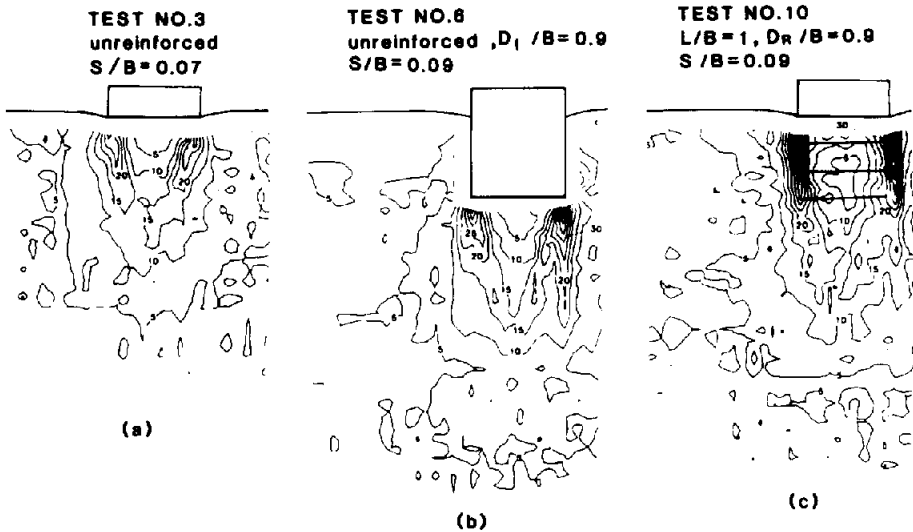


Fig. 5. Contours of $\epsilon_1 - \epsilon_3$ (%) for Group-a.

never mobilized simultaneously along the potential failure planes. This result also suggests that the most effective method of reinforcing is to place tensile reinforcement layers immediately beneath the footing so as to restrain the potential tensile strains as seen in Fig. 5(a).

Figure 5(b) is similar for a rigid deep footing of $D_f = 0.9B$ on unreinforced sand. In the zone beneath the footing, the pattern of strain distribution is similar to that seen in Fig. 5(a). Figure 5(c) is for the case of sand reinforced to a depth of $D_R = 0.9B$. The following points can be seen:

(a) In the zone reinforced to a depth of D_R beneath the footing, only small strains were induced. Along the lateral faces of this zone, intensely sheared bands were formed. These results indicate that the reinforced zone behaved like a part of rigid deep footing. This means that the potential strains, as seen in Fig. 5(a), had been restrained effectively and the shear bands formed in the unreinforced sand had moved outwards due to the effects of reinforcing.

(b) Beneath the reinforced zone, a largely strained zone was formed, and it is similar to that seen beneath the deep footing (Fig. 5(b)).

Figure 6(a) compares the normal stresses and the friction angles on the footing base at failure for sand either unreinforced or reinforced to different depths. It may be seen that the increase in the normal stress by reinforcing is larger at locations closer to the center of the footing. Typical examples of the relations between the shear stress on the footing base and settlement are shown in Figs 6(b) and (c). It may be seen that by

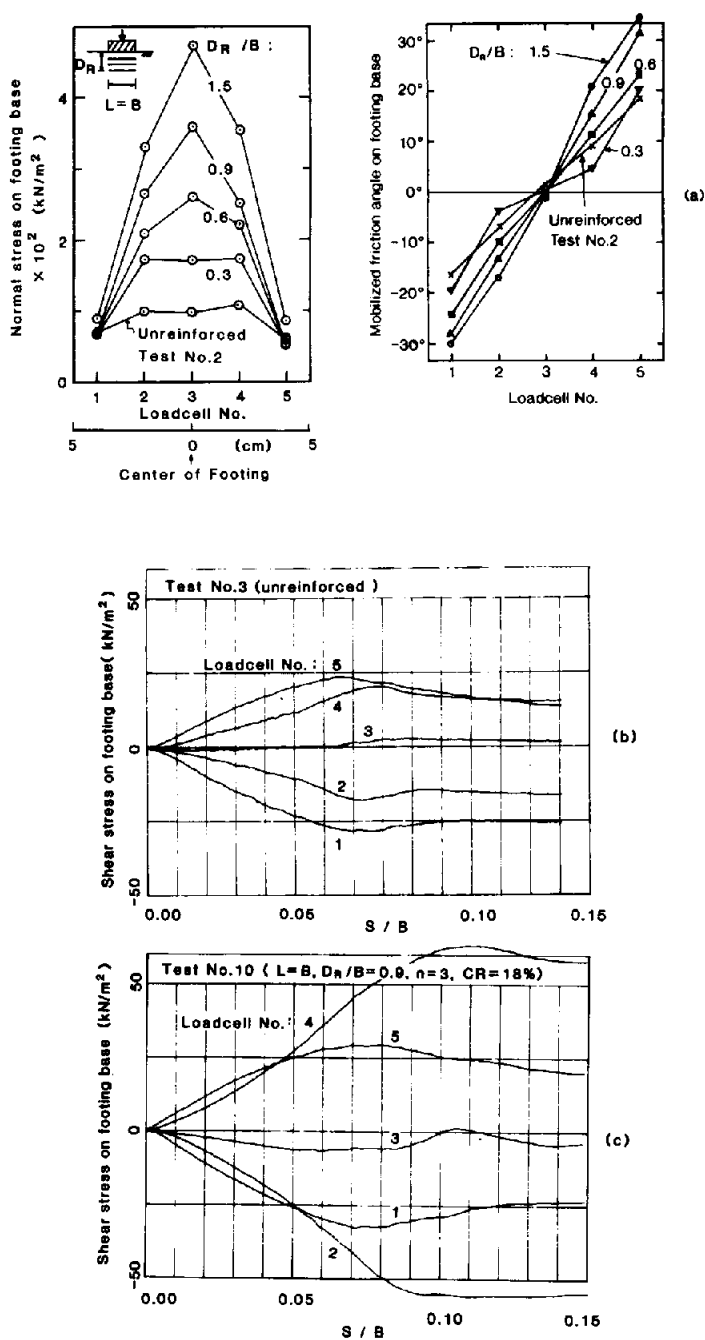


Fig. 6. Normal and shear stresses on footing base of surface footing on unreinforced and reinforced sand.

reinforcing, the shear forces became larger in load cells Nos 2 and 4, located at $0.2B$ from the center of the footing. These results suggest that the increased footing load by reinforcing to a depth is supported mainly by the increased compressive strength of the central part of the zone, which is a consequence of mobilized tensile forces in reinforcement. The strain-restraining failure mechanism³ for reinforced sand has been proposed based on these observations described above.

Consequently, it was concluded that ‘by densely reinforcing sand with stiff tensile-reinforcement having a length similar to the footing width, a failure occurs in sand beneath the reinforced zone, and the bearing capacity characteristics become very similar to that of unreinforced sand loaded with a rigid deep footing having an equivalent depth.’

3.2 Group-b

Figure 7 shows the footing load-settlement relationships for Group-b. In order to increase the bearing capacity, increasing the reinforcement

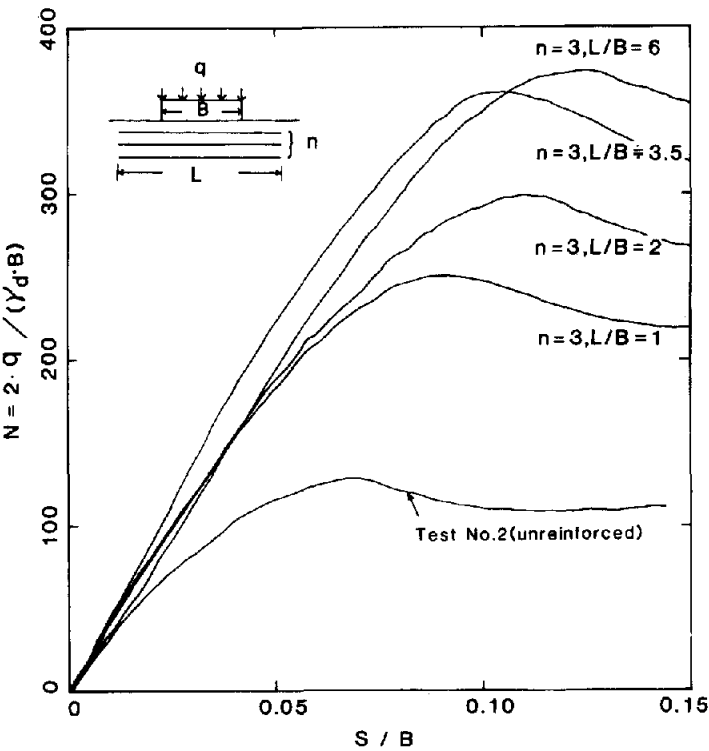


Fig. 7. Footing load-displacement relations for Group-b.

length L from B to $6B$ was found to be not as efficient as increasing the number of short reinforcement layers of $L = B$ as shown in Fig. 4. It is particularly true for the initial rigidity. Figures 8(a) and (b) show the measured tensile forces in reinforcement at steps with an increment of $S/B = 0.01$, for the cases of $L = 6B$ and $L = 3.5B$. It is seen that the tensile forces in reinforcement layers are largest at the center and much smaller outside the footing width. Furthermore, compressive forces were induced in some of the reinforcement members at about $1.25B$ from the center of footing. These results indicate the following two points:

(a) The effect of restraining the potential tensile strains is largest beneath the footing. The extended portions of reinforcement beyond the footing width contribute only in a secondary manner to the increase in the bearing capacity.

(b) The direction of reinforcement placed horizontally beyond $1.25B$ from the center of footing is very close to the direction of potential major principal strains in compression in unreinforced sand as observed in the present study. This means the reinforcing strips placed horizontally in that area cannot restrain potential tensile strains.

For different lengths of reinforcement, Figs 9(a), (b), (c) and (d) compare the strain fields at $S/B = 0.07$, at which the peak footing load is attained in the unreinforced sand loaded with a surface footing. Intensely sheared bands were formed along the vertical lateral faces of the reinforced zone with a width of $L = B$ (see also Fig. 5(a)). These were spread into wider areas by using reinforcement layers longer than B . This means that the zone reinforced with reinforcement layers longer than B behaved like a slab wider than B . Note also that the strain fields do not change largely for L equal to and larger than $2B$. Thus, the width of the 'wide slab' even for sand reinforced with very long reinforcement layers should not be considered equal to the length of reinforcement, but much smaller. Consequently, the increase in the bearing capacity by using long reinforcement layers can be considered due to the following two factors:

(a) The deep footing effect, as typically observed in the case of reinforcing with short reinforcement layers of $L = B$.

(b) The effects contributed by the portions of reinforcement placed in the zone beyond the footing width. This type of effect will be called the 'wide slab' effect. The effect increases at a smaller rate with the increase in L for L larger than B . The test results showed that the wide slab effect contributed by about 10 ~ 50% of the total increase in the bearing capacity and the degree of contribution increased with increasing CR or n , while slightly increasing with L when $L > 2B$.

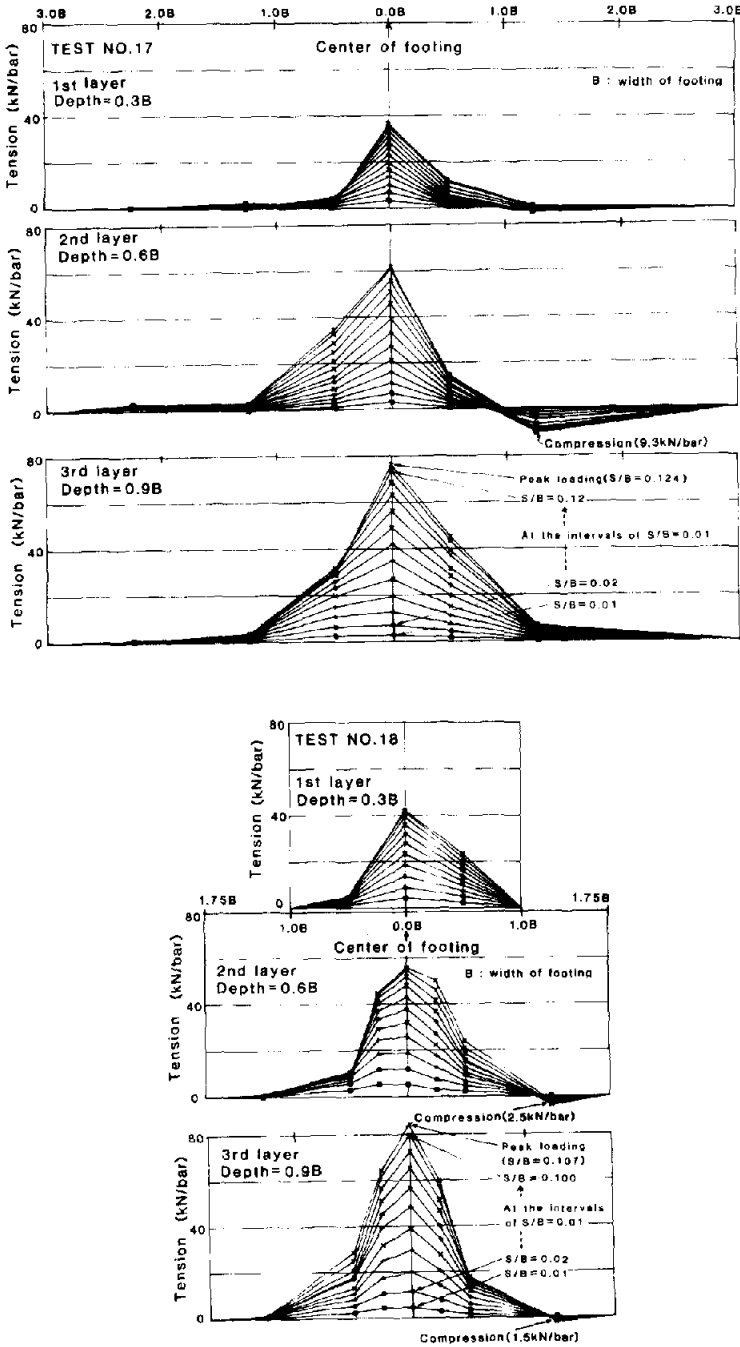


Fig. 8. Tensile forces in reinforcement up to peak. (a) Test No. 17 ($L/B = 6$, $n = 3$ and $CR = 18\%$); (b) Test No. 18 ($L/B = 3.5$, $n = 3$ and $CR = 18\%$).

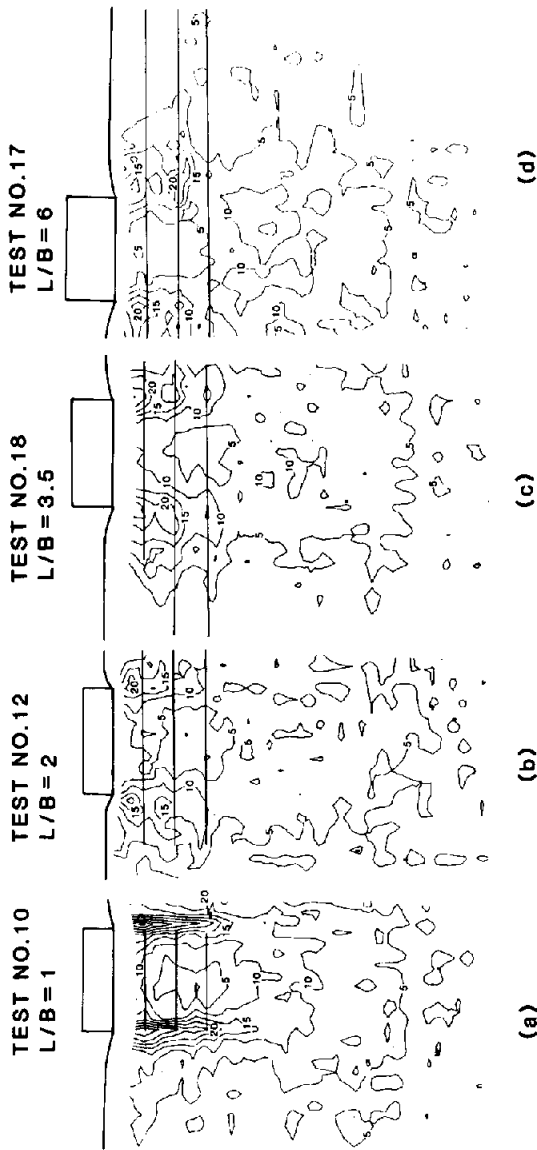


Fig. 9. Contours of $\epsilon_1 - \epsilon_3$ (%) for reinforced grounds in Group-b($D_f/B = 0.9$, $n = 3$ and $CR = 18\%$), $S/B = 0.0$ to 0.07 .

3.3 Group-c

Figure 10 compares the effects of the number of reinforcement layers n in the case of $L = 6B$. It may be seen that the bearing capacity increased with the increase in n in a manner quite similar to that observed for $L/B = 1$ in Group-a (see Fig. 4). This result also implies that the ‘deep footing effect’ is dominant also for reinforcement layers longer than B .

3.4 Group-d

Figure 11 shows the effects of covering ratio CR for the case of $L = 2B$ and $n = 3$. With increasing CR , both the peak strength and the settlement at peak load (S_f) increased. It may be noted that the increase in the bearing capacity was not proportional to CR for CR larger than 9%. This result suggests that there is an upper bound in CR , above which an increase in the bearing capacity with the increase in CR cannot be expected. This kind of

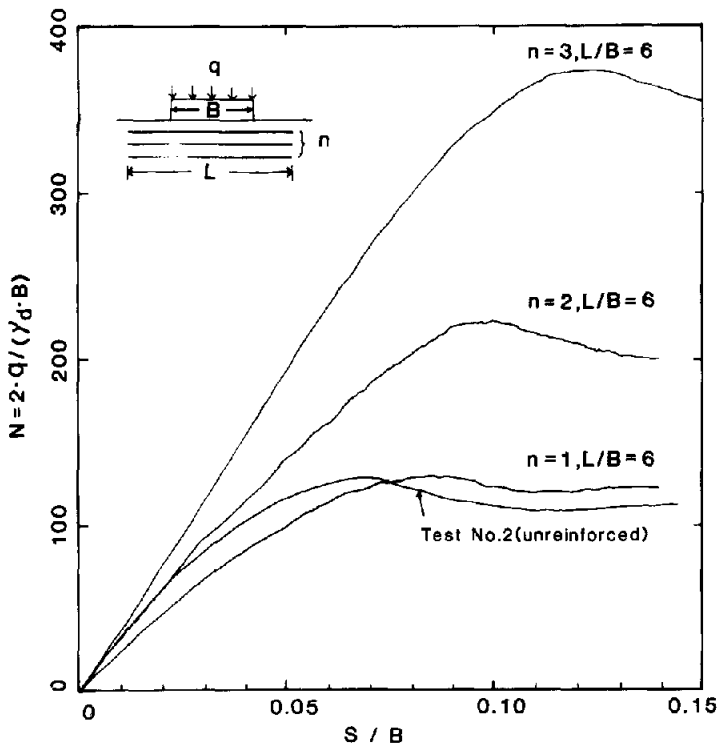


Fig. 10. Footing load-displacement relations for Group-c.

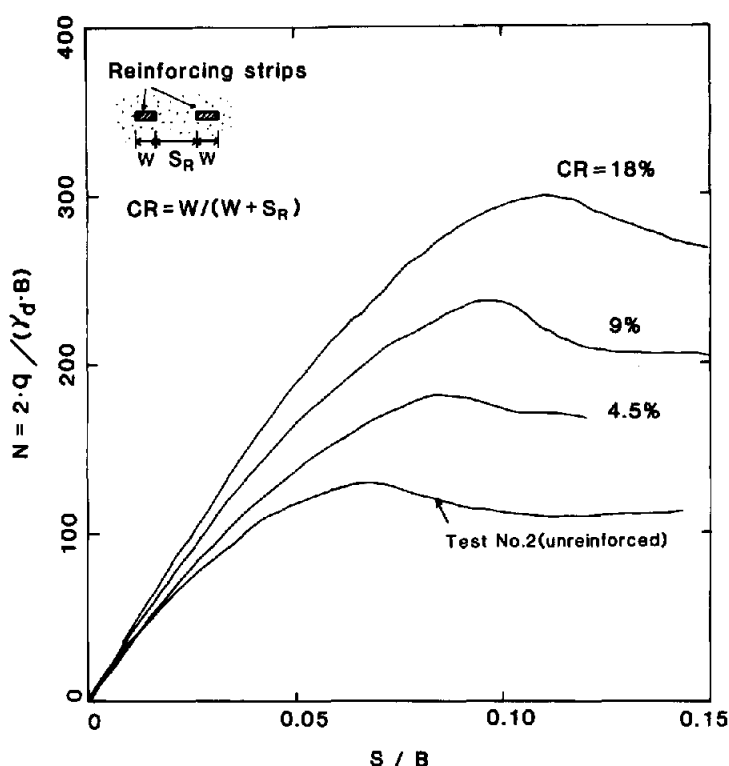


Fig. 11. Footing load-displacement relations for Group-d.

upper bound has been observed by Jewell⁷ in direct shear tests and by Tatsuoka⁸ in both PSC tests and bearing capacity model tests on reinforced sand.

Figures 12(a), (b) and (c) compare the strain fields. For the densely reinforced condition with $CR = 18\%$, immediately beneath the footing, a zone of small strain similar to that observed for $L = B$ in Fig. 5(b) may be clearly seen. However, for $CR = 4.5\%$, the strains in this zone were larger, while they were smaller than when unreinforced. This result indicates that failure tends to occur in the reinforced zone immediately beneath the footing when using a relatively small number of reinforcements.

3.5 Group-e

Fig. 13 shows the effects of the tensile rigidity and rupture strength of reinforcement. For the phosphor-bronze reinforcement of Types 2 and 3, the thickness of strip was different at 0.1 mm and 0.5 mm. The differences

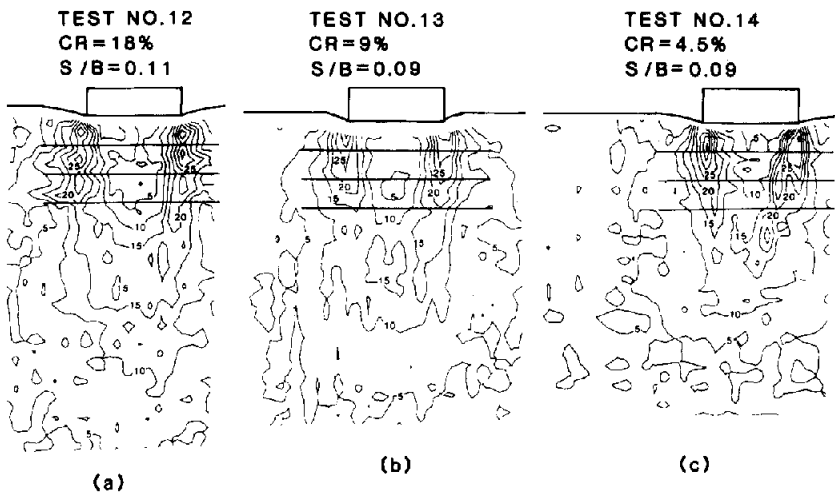


Fig. 12. Contours of $\epsilon_1 - \epsilon_3$ (%) for reinforced ground in Group-d($L/B = 2$, $D_R/B = 0.9$ and $n = 3$), $S/B = 0.00$ to S_f/B .

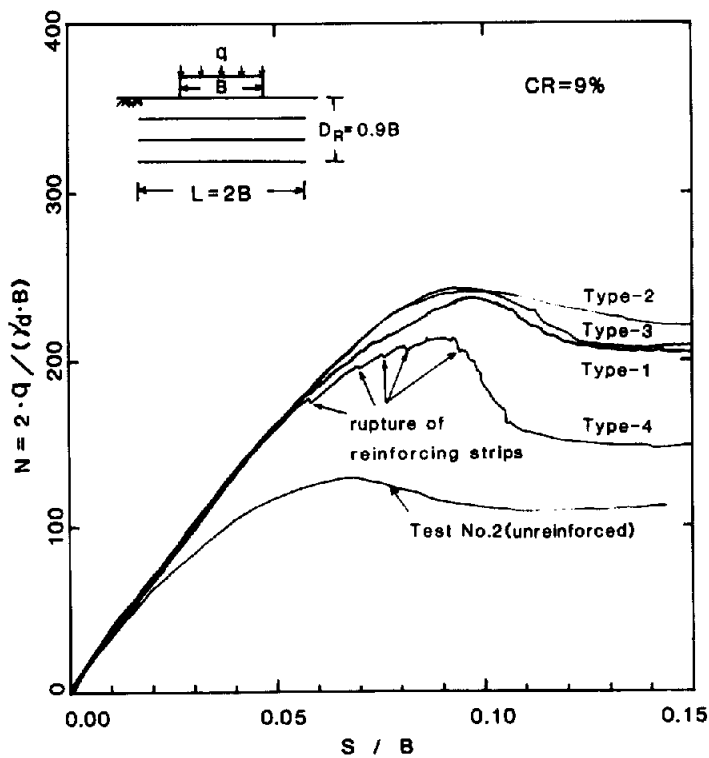


Fig. 13. Footing load-displacement relations for Group-e.

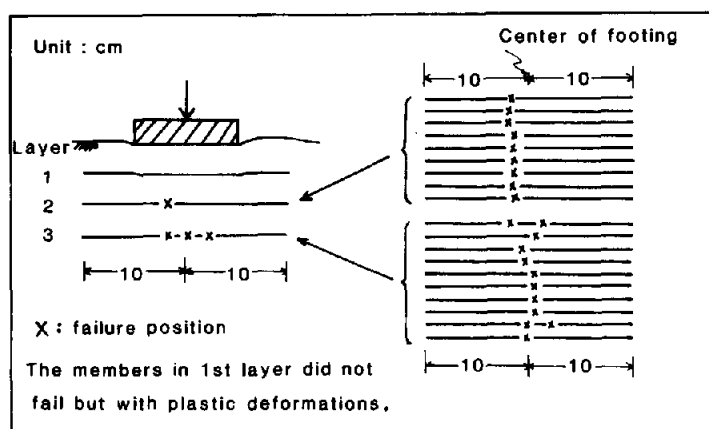


Fig. 14. Rupture of Type-4 reinforcement observed after the test.

in the bearing capacity of ground for the different tensile rigidity of reinforcement were negligible. Also for the case of Type-4 reinforcement, which had the smallest stiffness, the behavior was very similar to those for the other cases until the footing settlement S became approximately $0.06B$.

For Type 4, at S/B larger than 0.06 , the rate of the increase in the footing load decreased, accompanying fluctuation in the relationships. This behavior is due to the rupture failure of the reinforcement. The evidence is, first, the sound of rupture heard after $S/B = 0.06$ and as a more clear one, the breakage observed after excavating the model (Fig. 14). It is important to note that the failed positions in reinforcement are close to the central line of footing and a larger number of reinforcements failed at deeper layers. This result coincides with the measured tensile forces shown in Figs 8(a) and (b).

Note that among Types 2, 3 and 4, the tensile rigidities $E_R \cdot A_R$ were different by a factor of 17. These results indicate that unless the rupture failure of reinforcement occurred, the rigidity of reinforcement has negligible effects on the bearing capacity for the range examined in the present study. It is probable that the effects of reinforcement rigidity become pronounced only for a range of much smaller rigidities.

To make the surface of reinforcement very rough, sand particles were glued to the surface for Type-1 and ribs were attached for Type-2. The behavior for the two different surface conditions of reinforcement is also compared in Fig. 13. It may be seen that the difference is negligible. Thus, both types of reinforcement can be considered having similar very rough surfaces.

3.6 Failure mechanism for reinforced sand ground

From the test results, the failure modes in reinforced sand may be classified as follows:

(1) Compressive failure in the unreinforced zone beneath the reinforced zone as occurred in the unreinforced zone immediately beneath a rigid deep footing. This will be called 'Failure mode-1' as a result of the deep footing effect (Fig. 15(a)). For reinforcement having L larger than B , the contribution of the wide slab effect to the bearing capacity should be additionally accounted for.

(2) Compressive failure within the reinforced zone having a width similar to the footing width immediately beneath the footing, caused by an insufficient capability of reinforcement for restraining potential tensile strains in soil. It will be called 'Failure mode-2' (Fig. 15(b)). This type of failure results from one of the following factors: (a) the bond failure between sand and reinforcement surface; (b) an insufficient CR of reinforcement; and (c) the rupture failure of reinforcement. The compressive failure in reinforced zone due to the bond failure was not observed in the present study, while it may occur in the case of full-scale ground when the surface of reinforcement is not sufficiently rough.

4 MODEL FOR CALCULATING THE STRENGTH INCREASE IN REINFORCED SAND

4.1 Failure mode-1

It was found that when the value of ϕ at $\delta = 90^\circ$ by the PSC test (δ is the angle between σ_1 direction and the bedding plane) is used, the bearing capacity for unreinforced sand loaded with a surface footing is largely overestimated by a bearing capacity theory assuming the isotropic rigid-perfectly plastic properties for sand. For example, for Test No. 2, the bearing capacity factor N_γ calculated by using the equation of Meyerhof⁹ for $\phi = 49.4^\circ$ is 800. Compared with the measured value of 112, this theoretical value is extremely large. Such a discrepancy was found also for the bearing capacity factor N_q . This larger discrepancy is due mainly to the fact that the following two factors are ignored in the theory:

(1) Sand deposited vertically exhibits a large degree of anisotropy in its strength and deformation properties.^{4,5} Thus, the use of ϕ at $\delta = 90^\circ$ by a PSC test is an overestimation of ϕ in the ground in which the angle δ changes along potential failure planes.

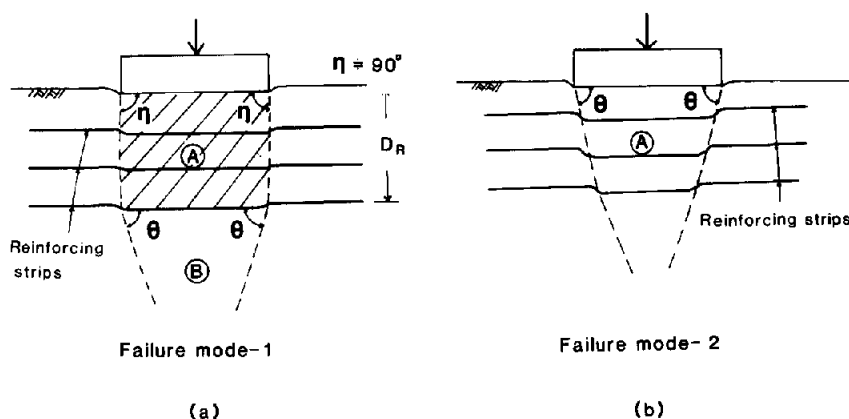


Fig. 15. Two failure modes of reinforced sand.

(2) As seen from Figs 5(a) and (b), the zone at and near failure is limited to the active zone immediately beneath the footing. This behavior is due to the progressive failure in ground.

Consequently, it was assumed that for a surface footing on unreinforced sand, the failure mode in the unreinforced block including the active zone is similar to that in a specimen for the PSC test as illustrated in Fig. 16(a). Then, the bearing capacity q_u may be obtained as:

$$q_u = q_1 + q_2 \quad (1)$$

in which q_1 is the compressive strength of the block and q_2 is the component by the other factors, such as the friction at lateral surfaces of the block and others, which do not exist in a PSC test. The value of q_1 was assumed to be obtained as:

$$q_1 = K_p \cdot \sigma_{cs}, \quad \sigma_{cs} = K_p \cdot \gamma_d \cdot (c + s_1)/2 \quad (2)$$

in which $K_p = \tan^2(45^\circ + \phi/2)$, ϕ is the internal friction angle of sand in the corresponding PSC test at $\delta = 90^\circ$, γ_d is the dry unit weight of sand, and c and s_1 are the height of the block and the settlement of footing at failure respectively.

A similar equation to eqn (1) was assumed valid for the bearing capacity q_B for unreinforced sand, loaded with a rigid deep footing:

$$q_B = q_3 + q_4 \quad (3)$$

in which q_3 is the compressive strength of the block including the active zone immediately beneath the deep footing (denoted by B in Fig. 16(b)),

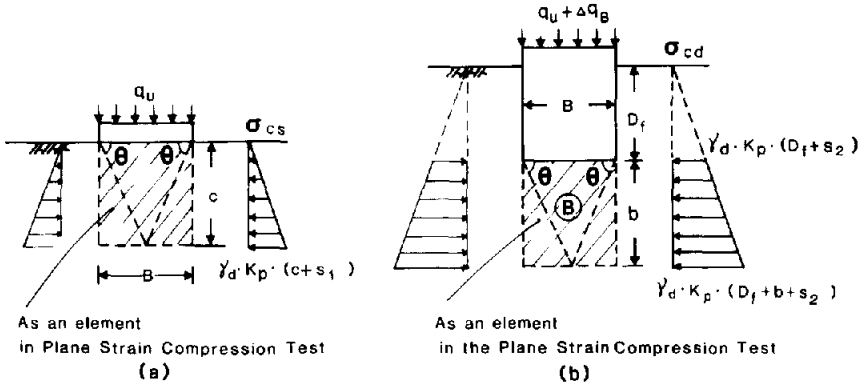


Fig. 16. Simplified failure modes for unreinforced ground; (a) surface footing, and (b) deep footing.

which also is considered to behave like an element in a PSC test, and q_4 is the component similar to q_2 , which does not exist in a PSC test. In the similar manner as for q_1 , the value of q_3 was assumed to be obtained as:

$$q_3 = K_p \cdot \sigma_{cd}, \quad \sigma_{cd} = K_p \cdot \gamma_d \cdot (2D_f + b + 2S_2)/2 \quad (4)$$

in which D_f , b and s_2 are the initial depth of footing, the height of the block B and the settlement of footing at failure, respectively.

The angle between shear band direction and the horizontal direction is denoted as θ in Fig. 16. The observed values of θ slightly scattered as $\theta = 45^\circ + \phi/2 + (3^\circ \sim 7^\circ)$, in which ϕ is the value estimated for each case and is in a range of $48.8^\circ \sim 50.2^\circ$. Since the effect of the small variation in θ on the results of analysis was found negligible, $\theta = 45^\circ + \phi/2$ was assumed in the following.

From eqns (1) and (3), the increase in the bearing capacity by deepening a rigid footing in unreinforced sand is obtained as

$$\Delta q_B = q_B - q_u = q_3 - q_1 + (q_4 - q_2) = q_3 - q_1 \quad (5)$$

Eqn (5) assumes that the term $q_4 - q_2$ is relatively small and can be neglected.

When reinforced sand loaded with a surface footing fails under Failure mode-1, the increase in the bearing capacity by reinforcing was assumed to be obtained also by eqn (5).

In the case of long reinforcement layers ($L > B$), the wide slab effect must be evaluated. One of the methods is to consider an equivalent rigid deep footing having a base wider than the original one. However, the

‘wide slab’ may be relatively flexible and may tend to deform nonuniformly, thus it may be difficult to evaluate the bearing capacity. Rather than that, the method used in the present study is to evaluate the increase in upward friction ΔS on the lateral surfaces of the zone directly beneath the footing (denoted as A in Fig. 17), induced by the tensile forces in reinforcement at its lateral surfaces. Thus, for Failure mode-1, the increase in the bearing capacity is obtained as:

$$\Delta q_C = \Delta q_B + \Delta S \quad (6)$$

in which Δq_B is obtained from eqn (5) and

$$\Delta S = 2 \cdot \left\{ \sum_{i=1}^n T_{e,i} \cdot \tan \phi \cdot N_i \right\} / B \quad (7)$$

in which n is the number of reinforcement layers, N_i is the number of reinforcements per unit length in the layer i and $T_{e,i}$ is the tensile force in each strip in the layer i at the lateral face of the block A. In the following analysis, for $T_{e,i}$, the values measured at the peak footing load, as shown in Figs 8(a) and (b), will be used. It is to be noted that in the case of $L = B$, Δq_C is equal to Δq_B .

4.2 Failure mode-2

For Failure mode-2, the increase in the compressive strength of the reinforced block A, shown in Fig. 18, will be denoted as Δq_A . It was assumed that Δq_A is due to the increase in the lateral confinement on block

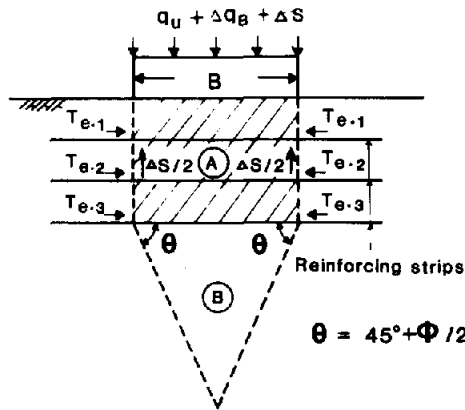


Fig. 17. Side wall friction for long reinforcement in Failure mode-1.

A, induced by tensile forces in reinforcement inside the block A. Thus, the value of Δq_A is obtained as:

$$\Delta q_A = K_p \cdot \sigma_t, \quad \sigma_t = \left\{ \sum_{i=1}^n (T_{av,i} \cdot N_i) \right\} / D_R \quad (8)$$

in which N_i is the number of strips per unit length in the reinforcement layer i , and $T_{av,i}$ is the averaged tensile force at the layer i in the block A. The value of $T_{av,i}$ was obtained as $(T_{max,i} + T_{e,i})/2$, in which $T_{max,i}$ and $T_{e,i}$ are the maximum tensile force at the center and the tensile force at the lateral surface of the block A in the strip i .

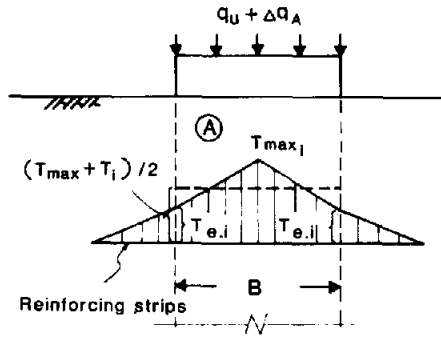


Fig. 18. Increase in confining pressure by reinforcing in Failure mode-2.

4.3 Comparisons between predicted and measured values

For obtaining the predicted values of the bearing capacity increase in reinforced sand, first, the value of Δq_A was compared with Δq_B or Δq_C for each case (Table 2). Then, the smaller value of these values was selected as a predicted value. The results of the analysis are shown in Figs 19–23, in which the bearing capacity increase in each case is presented in the normalized forms:

$$BCR = q_u(D_f > 0)/q_u, \quad BCR = q_u(D_R > 0)/q_u \quad \text{for measured values} \quad (9)$$

$$BCR_A = (q_u + \Delta q_A)/q_u$$

$$BCR_B = (q_u + \Delta q_B)/q_u$$

and

$$BCR_C = (q_u + \Delta q_C)/q_u \quad \text{for predicted values} \quad (10)$$

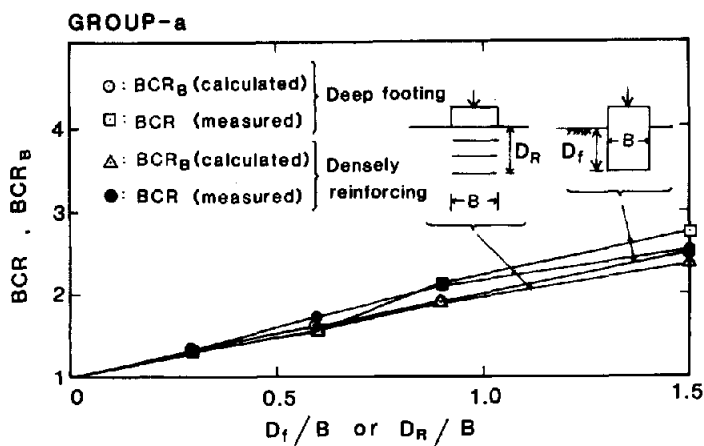


Fig. 19. Increase in bearing capacity by deepening a footing or by reinforcing with $L = B$ (Group-a).

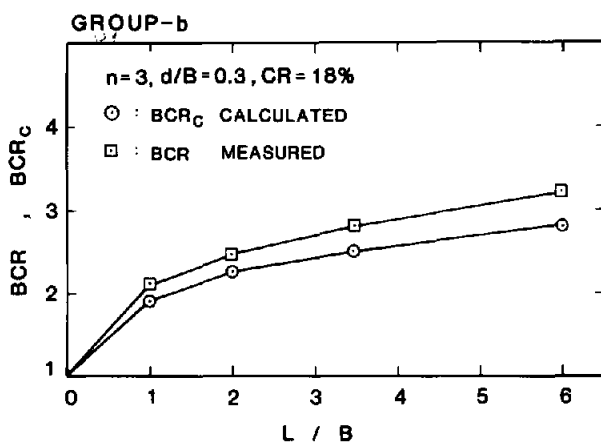


Fig. 20. Increase in bearing capacity by reinforcing plotted against L/B (Group-b).

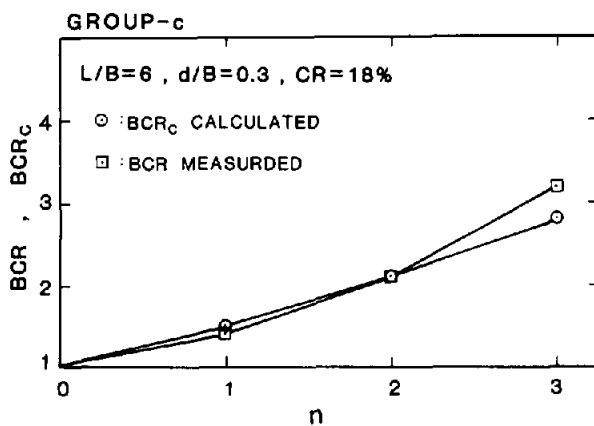


Fig. 21. Increase in bearing capacity by reinforcing plotted against n (Group-c).

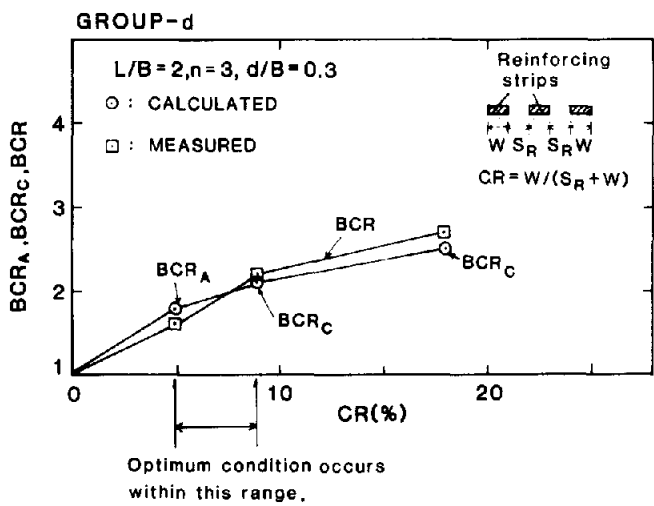


Fig. 22. Increase in bearing capacity by reinforcing plotted against CR (Group-d).

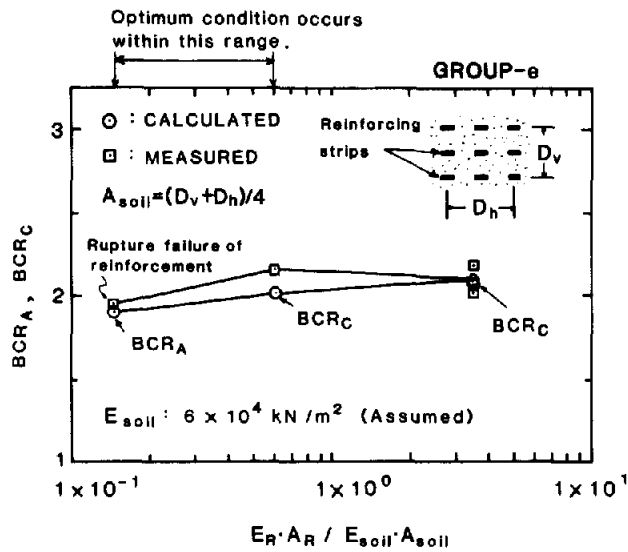


Fig. 23. Increase in bearing capacity by reinforcing plotted against tensile rigidity of reinforcement (Group-e).

in which q_u is obtained from the reference tests with a surface footing on unreinforced sand in Group-a, corrected to the same sand density for each case. $q_u(D_f > 0)$ and $q_u(D_R > 0)$ are the measured bearing capacity values for a deep footing in unreinforced sand and for a surface footing on reinforced sand, respectively.

It may be seen that the predicted values are well in accordance with the measured ones in all the cases, and the failure modes predicted also agree with observed ones.

In the present study, Failure mode-2 was observed and also predicted in two tests, which were:

(1) Test No. 14 in Group-d, in which the value of CR was insufficient and the rupture of reinforcement did not occur.

(2) Test No. 21 in Group-e, in which the rupture of reinforcement occurred. In this case, $T_{\max,i}$ in eqn (8) was assumed equal to the rupture strength.

When $\Delta q_A = \Delta q_c$, the arrangement of reinforcement can be considered as an optimum. It may be seen from Figs 22 and 23 that this condition may be realized between $CR = 4.5\%$ and 9% (Group-d) and between reinforcement Type-3 and Type-4 (Group-e).

5 TENSILE FORCES IN REINFORCEMENT

In the analyses described above, the measured tensile forces were used to predict the bearing capacity of reinforced sand. However, these values are to be estimated in design procedures. For obtaining information in this respect, the following analysis was made.

When the mobilized friction angle μ_{mob}^* and the normal stress σ_z^* on the surface of reinforcement at the moment of the peak footing load can be predicted, the shear stress or the bond stress τ can be calculated as

$$\tau = \sigma_z^* \cdot \tan \mu_{\text{mob}}^* \quad (11)$$

The tensile forces can be obtained by integrating τ . However, it is very difficult to estimate exact values of σ_z^* . Thus, it was assumed that the distributions of average vertical stress in the reinforced sand can be obtained from the elastic solution¹⁰ (Fig. 23);

$$\sigma_z = p \cdot \{\alpha + \sin \alpha \cdot \cos(\alpha + 2 \cdot \beta)\} / \pi \quad (12)$$

in which p is the contact normal stress on footing measured at the peak loading, as shown in Fig. 6(a), α and β are the angles shown in Fig. 24. The

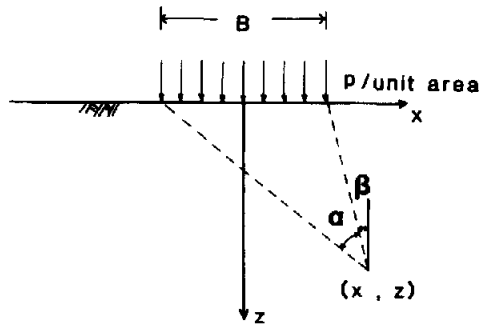


Fig. 24. Schematic figure of elastic solution for semi-infinite soil mass.

shear stress τ , on the surface of reinforcement measured at the peak load, averaged for a distance L , between the measuring points, No. i and No. $i + 1$, is expressed as,

$$\tau_i = (T_i - T_{i+1}) / (2 \cdot L_i \cdot W) \quad (13)$$

in which T_i and T_{i+1} are the measured tensile forces at No. i and No. $i + 1$ (see Fig. 8), and W is the width of reinforcement. Equation (13) assumes a linear variation in the tensile forces between the adjacent measuring points. Further, the shear stress along the reinforcement τ_a , averaged for a certain longer length $L_m = \sum L_i$, can be expressed as,

$$\tau_a = (\sum \tau_i \cdot L_i) / L_m \quad (14)$$

In the following analysis, when L is less than $2.5B$, $L_m = L/2$ was used. When L is not smaller than $2.5B$, $L_m = 1.25B$ was used. The values of σ_z averaged for L_m , σ_{za} , were obtained in a similar way. Then, the average mobilized friction angles for L_m were obtained as,

$$\mu_{\text{mob. a}} = \tan^{-1}(\tau_a / \sigma_{za}) \quad (15)$$

The values for both sides of the footing were averaged and plotted in Figs 25(a) and (b). Due to the several assumptions used, $\mu_{\text{mob. a}}$ calculated by eqn (15) should be considered as an approximation. It may be noted in Fig. 25(a) that the value of $\mu_{\text{mob. a}}$ for $D/B = 1.2$ was too small. It seems that this value is not very reliable, since the prediction of σ_z by eqn (12) becomes less accurate at deeper locations. The empirical relations shown

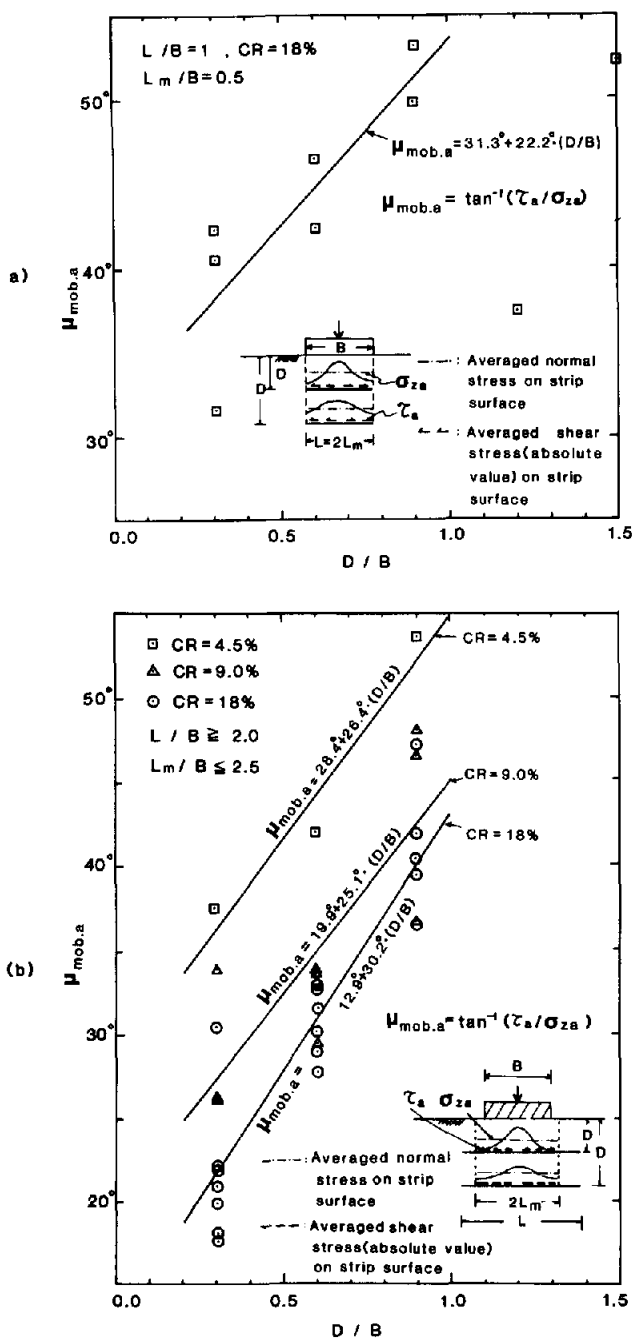


Fig. 25. Mobilized friction angles on reinforcement surface; (a) $L = B$; (b) $L \geq 2B$.

TABLE 3
Terms to be Checked when Designing a Soil-Reinforcement System

<i>Terms to be checked when designing a soil-reinforcement system</i>	<i>In strain-restraining mechanism^a</i>	<i>In anchoring mechanism^b</i>	
Equilibrium of boundary forces	Considered	Considered	
Local failure in reinforced zone	<div><div>Pull-out failure</div><div><div>Insufficient length</div><div>Bond failure between soil and reinforcement</div></div></div>	<div><div>Not considered, because it never occurs</div><div>Considered (did not occur in the present study)</div></div>	<div><div>Considered for the portions outside the shear bands (see Fig. 1)</div><div>Considered</div></div>
	<div><div>Compressive failure in soil</div></div>	<div><div>Considered</div><div>Considered</div></div>	<div><div>Not considered</div><div>Not considered</div></div>
	<div><div>Rupture failure of reinforcement</div></div>	<div><div>Considered</div></div>	<div><div>Considered</div></div>
	<div><div>Compressive failure in soil</div></div>	<div><div>Considered</div></div>	<div><div>Not considered</div></div>

^aFrom Huang & Tatsuoka (Ref. 3).

^bFrom Binquet & Lee (Refs 1, 2).

in the figures were obtained by the least square method. The following points may be seen:

(1) For both cases of $L/B = 1$ and $L/B > 1$, the friction angle $\mu_{\text{mob.a}}$ increases with the increase in the depth D of the reinforcement layer for which $\mu_{\text{mob.a}}$ is obtained, and is independent of the number of reinforcement layers.

(2) The friction angle $\mu_{\text{mob.a}}$ decreases with the increase in the covering ratio CR from 4.5% to 18%, but the decreasing rate between 9% and 18% is smaller than that between 4.5% and 9%. This tendency that the decrease in $\mu_{\text{mob.a}}$ as CR increases corresponds to the fact that the efficiency of increasing CR decreases as CR increases as shown in Fig. 11.

(3) For the same value of CR , the friction angle $\mu_{\text{mob.a}}$ is larger for $L/B = 1$ than for $L/B > 1$. This is due to the fact that the values of μ_{mob} outside the footing width are smaller than those within it.

Note that the largest value of the apparent friction angle $\mu_{\text{mob.a}}$ thus estimated is larger than 50° . This value may be much larger than the friction angle μ_{mob}^* , defined by using local stress σ_z^* (eqn 11). The difference is due to the stress concentration on the reinforcement surface, caused by the restraint to dilatancy as in the constant-volume simple-shear condition.

CONCLUSIONS

The test results of the present study show that the bearing capacity in sand can increase largely by reinforcing the zone immediately beneath the footing with stiff short reinforcement layers having only a length equal to the footing width. When densely reinforced, the reinforced zone behaved like a part of deep footing.

Based on the test results, a reasonably accurate method for predicting the bearing capacity increase in reinforced sandy ground was developed. The features of this method are summarized in Table 3. However, further studies on the mobilization of the friction angle between sand and reinforcement and the effect of the rigidity of reinforcement are needed. Also, in using this method, the large settlements which may occur at the peak footing load should not be ignored.

REFERENCES

1. Binquet, J. & Lee, K. L. Bearing capacity tests on reinforced earth slabs. *J. Geotech. Engng Div., ASCE*, **101**(GT12) (1975a) 1241–55.

2. Binquet, J. & Lee, K. L. Bearing capacity analysis of reinforced slabs. *J. Geotech. Engng Div., ASCE*, **101**(GT12) (1975b) 1257–76.
3. Huang, C. C. & Tatsuoka, F. Prediction of bearing capacity in level sandy ground reinforced with strip reinforcement. *Proc. Int. Geotech. Symp. Theory and Practice of Earth Reinforcement*, ed. Yamanouchi *et al.* Balkema, Rotterdam, 1988, pp. 191–196.
4. Tatsuoka, F., Molenkamp, F., Torii, T. & Hino, T. Behavior of lubrication layers of platens in element tests. *Soils and Foundations*, **24**(1) (1984) 113–28.
5. Tatsuoka, F., Sakamoto, M., Kawamura, T. & Fukushima, S. Strength and deformation characteristics of sand in plane strain compression at extremely low pressures. *Soils and Foundations*, **26**(1) (1986) 65–84.
6. Tatsuoka, F. Discussion on Paper by Bolton. *Geotechnique*, **37**(2) (1987) 219–25.
7. Jewell, R. A. Some effects of reinforcement on the mechanical behavior of soils. Ph D thesis, University of Cambridge, UK, 1980.
8. Tatsuoka, F. *Soil Reinforcing Method*. Japanese Society of SMFE (1986) pp. 25–165 (in Japanese).
9. Meyerhof, G. G. The ultimate bearing capacity of foundations, *Geotechnique*, **2** (1951) 301–32.
10. Poulos, H. G. & Davis, E. H. *Elastic Solutions for Soil and Rock Mechanics*. John Wiley & Sons, Inc., 1974, p. 36.